Optimizing Light Delivery to Perform Teleoperative Photoacoustic-Guided Hysterectomy

Gareth C. Keene[a] and Muyinatu A. Lediju Bell[a,b,c,d]

[a]Johns Hopkins University, Department of Electrical and Computer Engineering, Baltimore, MD
[b]Johns Hopkins University, Department of Computer Science, Baltimore, MD
[c]Johns Hopkins University, Department of Biomedical Engineering, Baltimore, MD
[d]Johns Hopkins University, Department of Oncology, Baltimore, MD

ABSTRACT

When designing an imaging system to perform photoacoustic-guided hysterectomy, one approach to achieve direct illumination of an imaging target is to attach optical fibers to the surgical tool. However, light blockage by the tool could potentially limit effectiveness. The work herein investigates optimal light delivery for a da Vinci surgical scissor tool. A tool tip located above a tissue surface was modeled with Monte Carlo simulations, and the resulting fluence was measured at the underlying tissue surface and 1 mm below the tissue surface. A design was prototyped and built based on the simulation results, and the corresponding light profiles were compared to theoretical calculations based on optical parameters and geometry. The simulated fluence measurements located 1 mm below the tissue surface were maximized with an optical fiber directing light 15° toward the tool shaft at a 12.7 mm separation distance between the fiber and the tool shaft, offering 29-48% improvement relative to 0° skew and 0.2 mm tool shaft-to-fiber separation distance, as a function of tool tip-to-tisssue surface distances of 0-17 mm. After thresholding the simulated fluence at the illumination surface by 1/e of its maximum value, the simulated light profiles had similar shapes to the corresponding experimental profiles, demonstrating a reduction in the shadow caused by light blockage observed with the optimal design (relative to that achieved with the original design). The outer diameters of the 1/e thresholded simulated light profile and the corresponding theoretical surface profile agreed within 6-7%. These findings are promising to maximize light delivery in both robotic and nonrobotic photoacoustic-guided hysterectomies (as well as other surgeries that utilize minimally invasive tools), which has the potential to provide surgeons with more precise situational awareness.

1. INTRODUCTION

Photoacoustic-guided surgical procedures have emerged as a promising approach in minimally invasive surgeries, offering real-time visualization of tissue structures without the use of ionizing radiation.[1–4] These procedures combine the benefits of optical imaging and ultrasound, providing high-contrast, depth-resolved images of biological tissues. As the medical community continues to prioritize minimally invasive techniques under the principle of "first, do no harm," the integration of photoacoustic imaging in surgical workflows has become increasingly relevant. Surgeries have successfully achieved minimal invasiveness through laparoscopy, which utilizes tools and illumination devices to visualize and operate inside the abdomen without creating large incisions.[5] This approach has significantly reduced patient recovery times and complications. However, the risk for injury during a laparoscopic procedure is greater in the presence of co-morbidities, including endometriosis in the case of laparoscopic hysterectomies.[6]

Robot-assisted hysterectomy procedures have become increasingly popular with the da Vinci surgical system, due to greater dexterity and stereoscopic imaging capabilities resulting in fewer malign complications, quicker recovery times, and shorter hospital stays compared to laparascopy.[7] While injury rates have decreased due to the introduction of robotic assistance, procedures significantly concealed by tissue still present a greater challenge for safe operation when compared to standard cases without problematic concealing tissue.[6] This obstacle to safe operation suggests that there is room for improvement through the inclusion of robust imaging techniques with the ability to display information about targets underlying tissue.

Photons Plus Ultrasound: Imaging and Sensing 2025, edited by Alexander A. Oraevsky, Lihong V. Wang, Proc. of SPIE Vol. 13319, 133190E · © 2025 SPIE
1605-7422 · doi: 10.1117/12.3044905

Photoacoustic imaging offers a portable solution to distinguish various tissues due to differences in optical absorption.[1] This imaging approach operates by sending pulsed laser signals toward a target of interest. The laser pulses are selectively absorbed by the target, thus causing periodic isometric expansion and contraction in the target, which in turn causes omnidirectional acoustic pressure to propagate from the target toward an ultrasound transducer that detects the signal for reconstruction of the target location. Light delivery for photoacoustic-guided surgical procedures could be implemented by attaching the optical fibers to the ultrasound transducer.[8,9] However, this setup unnecessarily complicates localization of surgical tool tips relative to critical structures of interest in a photoacoustic image.[8]

An innovative approach that attaches optical fibers directly to the surgical tool enables illumination of the tool tip relative to a critical structure in the same photoacoustic image.[1] Initial designs of this novel concept were developed for minimally invasive neurosurgery,[2] determining that seven optical fibers were optimal. Using fewer optical fibers created disconnected optical profiles at the illumination surface, while additional optical fibers did not increase the illumination area.

When translating this approach to da Vinci surgical tools, initial demonstrations revealed promise to visualize blood vessel structures.[10] However, various tool tip orientations absorbed a significant component of the transmitted light profile, causing "shadows" on the incident tissue, which ultimately prevent the desired fluence from reaching the area directly beneath the tool tip.[3] This limitation affects the quality and consistency of photoacoustic images, with tool orientation differences responsible for >5 dB contrast reduction at 15 mm distance from the photoacoustic target when scissor blades were open rather than closed.[3] We anticipate that there is an optimal set of physical parameters for a prototype fiber holder that will minimize shadows and thereby optimize optical fluence for surgical guidance.

The purpose of the work herein is to design a light delivery approach that will reduce optical shadows, minimize fluctuations in the resulting light profile, and maximize light delivery to tissues beneath tool tips to visualize critical structures hidden by tissue. To achieve these objectives, the presented work has three integrated components. First, an elliptical tool model with matching physical parameters of the surgical tool was simulated,[11] followed by comparisons of measured fluence. Second, a physical prototype (hereafter referred to as the optimized holder) was designed and built based on the optimal parameters determined with simulations. Third, expected improvements (e.g., shadow reductions, greater fluence) in the light profile produced by the optimized fiber holder were experimentally validated and compared with predictions from theory and simulations.

2. METHODS

2.1 Theoretical Light Profile Calculations

To predict the area of the light profile beneath the tool tip on the tissue surface for comparison with the simulation and experimental results, geometric approximations were performed using the numerical aperture of the optical fibers. The tool geometry and fiber tips were plotted to determine the angle of marginal rays (i.e., rays that travel closest to the tool tip while still reaching the tissue below as depicted in Fig. 1) for the original and optimized parameters. The intersection of the marginal rays with the tool were calculated by finding the line connecting the origin point of the optical fiber tangentially to the edge of the ellipse model of the tool, performed using Desmos (Desmos Studio, Beaverton, Oregon).

For the original fiber holder, the marginal ray is approximately normal to the tissue surface. Thus, the area of the light profile illuminating an underlying surface is given by:

$$A_{original} = \pi((d+r)^2 - r^2), \tag{1}$$

where d is the distance between the light source and the outer edge of the light profile on the illumination surface and r is the distance between the center of the tool and the light source.

The marginal ray for the optimized holder propagates at an angle θ relative to a line normal to the tissue surface and intersects the tool axis at a distance defined as $s_{critical}$ below the tool. A ray traveling from another location will also cross the tool axis at the same value of $s_{critical}$. Therefore, a shadow resulting from occlusion of light by the tool will exist if $s < s_{critical}$. When $s \geq s_{critical}$, the corresponding area calculation ignores the

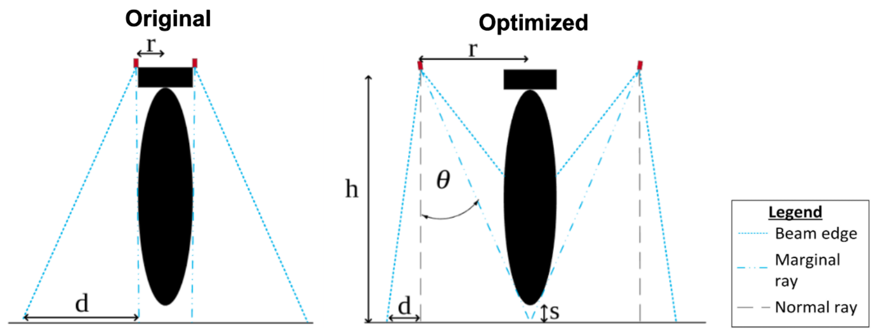

(a) (b)

Figure 1: Schematic diagrams of fiber holders and associated light profile geometries expected with (a) original and (b) optimized (as described in Section 2.2) parameters, where $r = 4$ mm and 16.7 mm for the original and optimized fiber holder, respectively, and $d = 21.2$ mm and 7.03 mm for the original and optimized fiber holder, respectively, s ranges from 0 to 17 mm, $h = s +$ the length of the tool tip (i.e., 33 mm), and $\theta = 25.4°$.

term that factors in the shadow, due to the marginal rays from opposite sides overlapping and eliminating a geometric basis for an internal shadow, described as follows:

$$A_{optimized} = \begin{cases} \pi((d+r)^2 - (r - h\tan\theta)^2), & \text{if } s < s_{critical} \\ \pi(d+r)^2, & \text{if } s \geq s_{critical} \end{cases} \tag{2}$$

where s is the distance from the tool tip to the illumination surface, h is the distance between the light source and the illumination surface, and θ is the angle between the normal and marginal rays. Based on the optimized fiber holder parameters (determined as described in Section 2.2), $s_{critical} = 2.2$ mm.

2.2 Monte Carlo Simulations

A tool tip was modeled using the Monte Carlo eXtreme (MCX) software,[13] which uses the Monte Carlo statistical method to simulate numerous light rays interacting with turbid media. Fig. 2(a) shows a close-up of the da Vinci monopolar scissors tool alongside an image displaying the tool with the original fiber holder and laser fibers attached (Fig. 2(b)). The optical simulation software does not support native CAD models, necessitating shapes to be defined manually. Therefore, the da Vinci scissors tool was represented as an ellipse using the length (33 mm) and width (8 mm) parameters shown in Fig. 2(a), resulting in the model shown in Fig. 2(c).

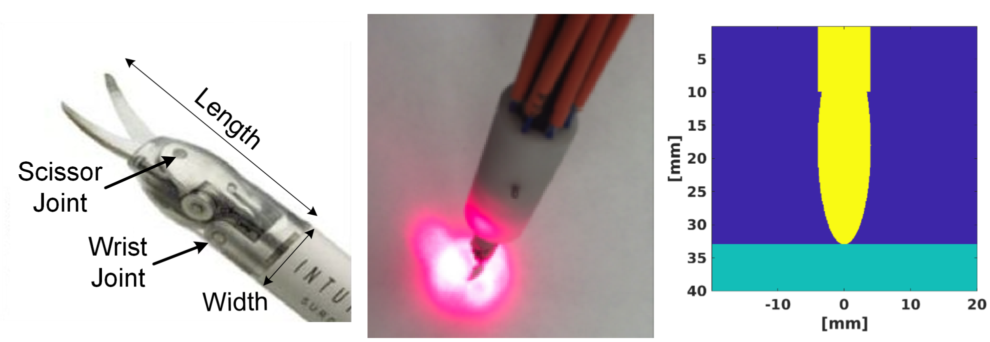

(a) (b) (c)

Figure 2: (a) Annotated photograph of the da Vinci monopolar scissors tool,[12] (b) da Vinci monopolar curved scissors with the original fiber holder attached, demonstrating the associated light profile produced,[3] and (c) elliptical representation of the monopolar scissors tool in the Monte Carlo eXtreme (MCX) simulation environment.

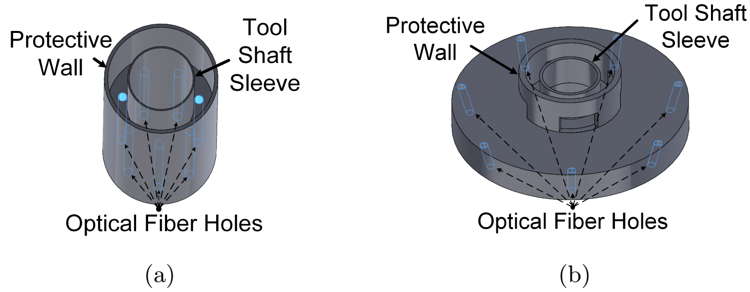

Figure 3: SolidWorks models of (a) original and (b) optimized fiber holders. Key features include holes to align optical fibers (blue), central flexible sleeve for tool shaft grip, protective wall, and angled holes in the optimized design.

Table 1: Fundamental dimensions and design parameters of the original and optimized fiber holders

	Original Fiber Holder	**Optimized Fiber Holder**
Diameter	16 mm	37.2 mm
Height	39.2 mm	11.4 mm
Optical Fiber Hole Width	1.2 mm	1.2 mm

The scattering coefficients, absorption coefficients, and anisotropy factors associated with 750 nm optical wavelength[14,15] were utilized. Five parameters were varied after defining the tool properties: (1) wrist joint rotation, (2) scissors joint rotation, (3) vertical displacement from tissue, (4) angular skew of optical fibers relative to the tool shaft, and (5) lateral displacement of optical fibers relative to the tool shaft.

Fluence at the illumination surface was thresholded at 1/e of the maximum fluence to calculate the surface area of the light profile, with the distance between the tool tip and tissue surface ranging from 0 to 17 mm. In addition, a circular region of interest (ROI) with a 10 mm radius located perpendicular to tool axis, 1 mm below the tissue surface, and at the lateral center of the tissue model, was defined to quantify fluence. The tool distance from the tissue surface was 2 mm. Fluence within the ROI was measured as two parameters anticipated to be most influential (i.e., the light source skew from the axis of the tool shaft and the lateral displacement from the tool shaft perimeter) were varied across 176 permutations. The permutations ranged from -32.5° skew (where 0° is parallel to the tool axis) and 0.2 mm lateral separation from the tool shaft perimeter to 5° skew and 25.2 mm lateral separation, incremented by 2.5° and 2.5 mm, respectively.

2.3 Optimized Holder Design and Fabrication

A SolidWorks (Waltham, MA) model was designed, based on the optimal parameters identified with simulations, to accommodate seven fibers surrounding a da Vinci monopolar scissors tool. Relative to the previous fiber holder (Fig. 3(a)), the optimized holder (Fig. 3(b)) features angled holes to skew the optical fibers relative to the tool shaft. As in the previous design, a central hole with a flexible sleeve was incorporated to grip the tool shaft, surrounded by a protective wall to prevent damage to the sleeve. A physical prototype based on the new design was then created using a FormLabs 3B+ stereolithography 3D printing machine (Somerville, MA) with Grey Resin V4. Table 1 summarizes the dimensions of the original and optimized fiber holders.

2.4 Experimental Validation

To experimentally validate the optimized holder, the tip of a da Vinci monopolar curved scissors tool and seven surrounding optical fibers were inserted into designated locations within the optimized holder. The associated 1-to-7 fiber splitter was modified from the Thorlabs (Newton, NJ) BF76LS01 commercially available product. The setup was positioned orthogonal to a sheet of graph paper to measure resulting light profiles from the opposite side of the sheet, as shown in Fig. 4. This procedure was implemented to measure the light profiles produced by the original fiber holder, employed in previous research,[3] (Fig. 4(a)) and the optimized fiber holder (Fig. 4(b)).

To photograph light profiles produced by the optimized holder and its predecessor, each design was connected to a 690 nm wavelength pulsed laser source with 10 Hz pulse repetition frequency (Opotek, PhocusMobile,

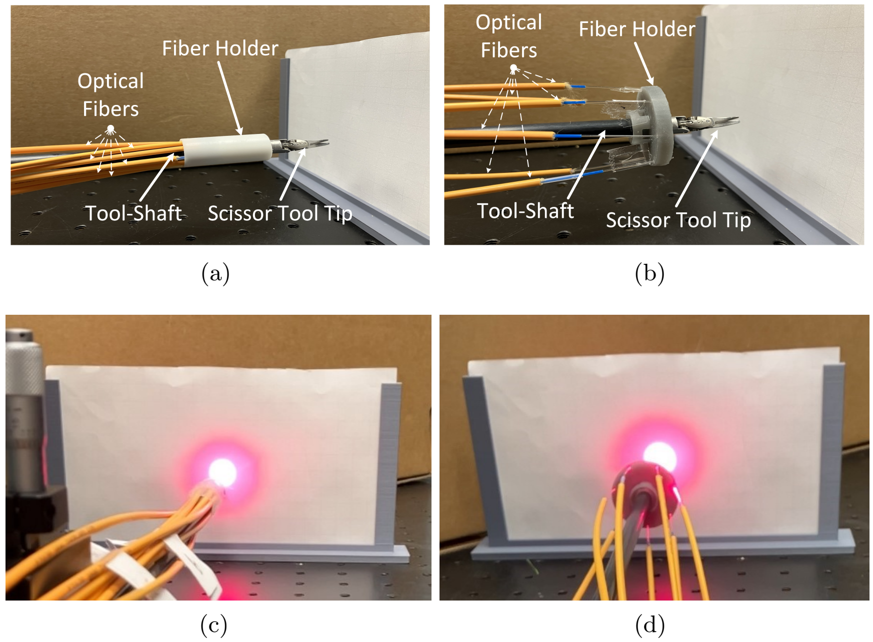

Figure 4: Experimental setup to compare the light profiles from the (a,c) original and (b,d) optimized fiber holders in the (a,b) absence and (c,d) presence of transmitted light.

Carlsbad, CA, USA). The chosen laser wavelength differed from the 750 nm wavelength employed in simulations to maximize profile visibility in photographs. The mean energy measured at the output of the seven fibers without either fiber holder was 1.4 mJ per pulse. The profiles illuminating the graph paper in the photographs were measured and compared to corresponding profiles obtained from simulations. These experiments were performed in a dark room (e.g., overhead room lights were off and a blackout curtain was drawn).

3. RESULTS

Fig. 5 shows the fluence measured 1 mm below the tissue surface when varying the simulation parameters of skew and lateral shift relative to the tool shaft. With 15° skew toward the shaft and 12.7 mm of shift away from the shaft (indicated by the red box in Fig. 5), fluence increased by 29% relative to that of the original fiber

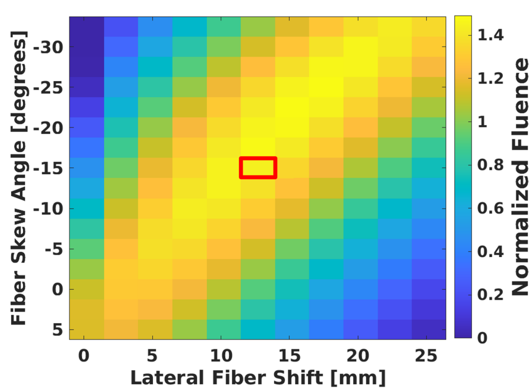

Figure 5: Fluence measured 1 mm below the tissue surface with the tool tip located 2 mm above the tissue surface, as a function of 176 combinations of fiber skew and shift. The selected optimal normalized fluence value (red box) corresponds to -15° angular skew and 12.7 mm lateral shift relative to the tool shaft, defining chosen parameters for the optimized fiber holder.

holder parameters, when the tool-to-tissue separation distance was $s = 2$ mm. These parameters were used to design the physical prototype of the optimized holder. At tool-to-tissue separation distances of 0-17 mm, the fluence improvement achieved with the optimized parameters ranged 29-48%.

Fig. 6 shows simulated and experimental light profiles obtained with the original and optimized light delivery designs, with the tool tip placed 17 mm from the illumination surface in each case. With the original design parameters, the circular shadow caused by light blockage was 6 mm in diameter, as assessed with thresholding at 1/e of the maximum simulated fluence amplitude (Fig. 6(a)). This circular shadow was mitigated in simulations with the new (i.e., optimized) design in (Fig. 6(b)), based on the same 1/e threshold applied to the corresponding normalized fluence measurements. The boundaries obtained with the simulated result, at a threshold of 1/e of the maximum fluence are overlaid on the corresponding experimental results in Fig. 6, after reducing the scale of the boundaries by a factor of 3 to support the observation that the optimized fiber holder parameters mitigate the light profile shadow observed with the original parameters, resulting in a more uniform optical profile near the tool tip.

Fig. 7 shows photographs of the experimental light profiles obtained with the original and optimized fiber holders, when the tool was located at a distance of 17 mm from the illumination surface (i.e., the measuring sheet in Fig. 4). The outer boundaries of the simulated and theoretical light profiles obtained at the same

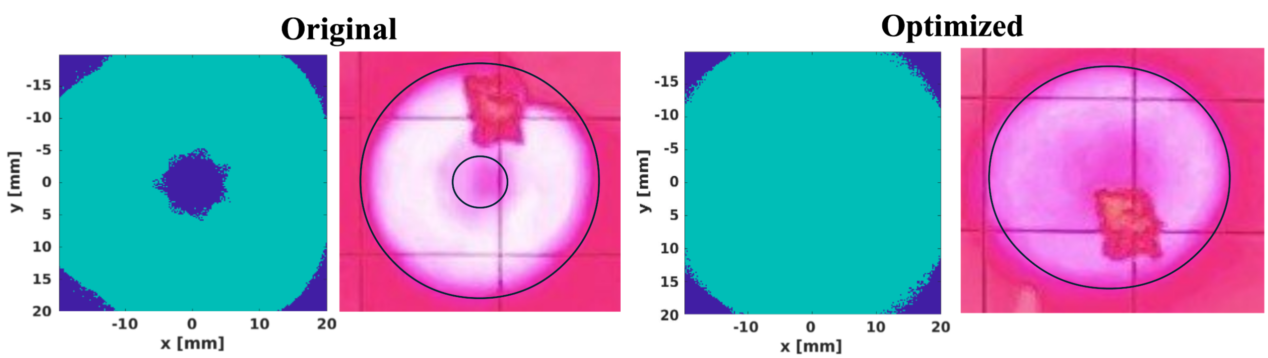

(a) (b)

Figure 6: Pairs of (left) simulated fluence results, after thresholding to 1/e of the maximum fluence, and (right) experimental light profile results obtained with the parameters of the (a) original and (b) optimized fiber holders. The circles overlaid on the experimental photographs correspond to the borders of the simulated images (after reducing the boundaries obtained with the 1/e fluence threshold by a factor of 3), included to demonstrate the similarity between simulated and experimental results. The mark in each experimental photograph denotes the tool axis.

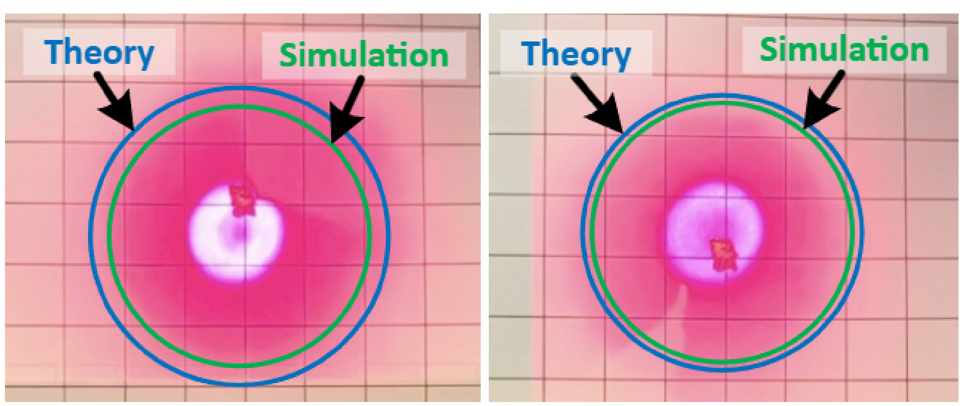

(a) (b)

Figure 7: Simulated and theoretical light profile boundaries obtained with the (a) original and (b) optimized fiber holders, overlaid on experimental photographs (with marks denoting the tool axis).

distance from the illumination surface, based on the simulated results in Fig. 6 and the geometry shown in Fig. 1, respectively, were overlaid on the experimental light profiles. After 1/e thresholding, the simulated outer diameters of the light profiles obtained with the original and optimized fiber holders were 46.9 mm and 44.9 mm, respectively, representing a 6-7% difference from theory, as reported in Table 2. The corresponding light profile areas and associated percent differences are also reported in Table 2. The smaller area achieved with the optimized fiber holder is likely responsible for the greater fluence measured with the corresponding simulation.

Table 2: Simulated and theoretical light profile boundaries and areas obtained with the original and optimized fiber holders, located 17 mm from the tissue surface, with corresponding percent differences relative to the theoretical predictions.

		Theory	**Simulation**	**% Difference**
Outer Diameter	Original	50.4 mm	46.9 mm	7%
	Optimized	47.5 mm	44.9 mm	6%
Area	Original	1945 mm^2	1708 mm^2	12%
	Optimized	1769 mm^2	1581 mm^2	11%

4. DISCUSSION

This work is the first to investigate the optimal arrangement of optical fibers surrounding a da Vinci scissor tool. The greater uniformity of the light profile produced by the optimized fiber holder simplifies our understanding and delivery of the minimum laser energy needed to visualize a structure (e.g., by avoiding "hot spots" in a laser profile, which can potentially be damaging to tissue[2]). The recovery of accurate chromophore distributions is additionally expected to be less complicated when fluence is uniform across an ROI.[16]

The optimized tool prototype has a diameter of 37.2 mm. While the largest known trocar to accept da Vinci tools for insertion into the body has a diameter of 12 mm,[17] our prototype can be further minimized by beveling fibers[18–20] or using galvo mirrors[21,22] to place the light profiles at the intended distances from the tool shaft. Future designs might also incorporate a dynamic extension mechanism to extend the light sources after insertion of the tool through the trocar (i.e., within an insufflated abdomen).

The marks demonstrating the tool axis are notably off-centered from the center of the light profiles in Figs. 6 and 7. This misalignment is likely due to varying levels of tension in the individual optical fibers during data acquisition. Hence, this misalignment was ignored when providing demonstrations of the similarity between experimental profiles with the predictions from theoretical and simulated data, which were demonstrated under the assumptions of otherwise concentric optical profiles.

One potential limitation with regard to extensions to future work is that the tool modeling method presented in Section 2.2 used graphical equations to represent the monopolar scissors as an ellipsoid. While the corresponding results were validated with experimental light profiles achieved with a da Vinci curved scissor tool, other da Vinci surgical tools may have more complex shapes. The modeling of light profiles for these more complex shapes may benefit from importing computer-aided design (e.g., SolidWorks) models into a Monte Carlo software that supports such models (e.g., mesh-based Monte Carlo[23]). Despite this limitation, the success of our optical modeling approach indicates translatability and generalizability to optimize light delivery for other surgical tool tips. Hence, these results are promising to maximize light delivery in both robotic and nonrobotic photoacoustic-guided hysterectomies (and other surgeries that utilize minimally invasive tools).

5. CONCLUSION

The research presented herein investigates light delivery in photoacoustic-guided surgeries with a da Vinci surgical scissors tool with attached optical fibers. Based on simulations with tool-to-tissue distances ranging 0-17 mm, the fluence delivered below the tool improved by 29-48% relative to that of the original holder. The optimized fiber holder design additionally mitigated the shadow artifact observed with simulated and experimental results. Simulated and theoretical light profile diameters differed by 6-7%. These improvements promise greater situational awareness during photoacoustic-guided surgeries (e.g., hysterectomies).

ACKNOWLEDGMENTS

This work is supported by NIH R01 EB032358.

REFERENCES

[1] M. A. L. Bell, "Photoacoustic imaging for surgical guidance: principles, applications, and outlook," *Journal of Applied Physics* **128**(6), 060904 (2020).

[2] B. Eddins and M. A. L. Bell, "Design of a multifiber light delivery system for photoacoustic-guided surgery," *Journal of Biomedical Optics* **22**(4), 041011 (2017).

[3] M. Allard, J. Shubert, and M. A. L. Bell, "Feasibility of photoacoustic-guided teleoperated hysterectomies," *Journal of Medical Imaging* **5**(2), 021213 (2018).

[4] E. A. González, A. Jain, and M. A. L. Bell, "Combined ultrasound and photoacoustic image guidance of spinal pedicle cannulation demonstrated with intact ex vivo specimens," *IEEE Transactions on Biomedical Engineering* **68**(8), 2479–2489 (2021).

[5] I. Alkatout, U. Mechler, L. Mettler, *et al.*, "The development of laparoscopy—a historical overview," *Frontiers in surgery* **8**, 799442 (2021).

[6] S. E. Delacroix and J. Winters, "Urinary tract injuries: recognition and management," *Clinics in colon and rectal surgery* **23**(03), 221–221 (2010).

[7] S. Maeso, M. Reza, J. A. Mayol, *et al.*, "Efficacy of the da vinci surgical system in abdominal surgery compared with that of laparoscopy: a systematic review and meta-analysis," *Annals of surgery* **252**(2), 254–262 (2010).

[8] S. Gao, Y. Wang, X. Ma, *et al.*, "Intraoperative laparoscopic photoacoustic image guidance system in the da vinci surgical system," *Biomed. Opt. Express* **14**, 4914–4928 (2023).

[9] H. Moradi, E. M. Boctor, and S. E. Salcudean, "Robot-assisted image guidance for prostate nerve-sparing surgery," in *2020 IEEE International Ultrasonics Symposium (IUS)*, 1–3 (2020).

[10] N. Gandhi, M. Allard, S. Kim, *et al.*, "Photoacoustic-based approach to surgical guidance performed with and without a da vinci robot," *Journal of Biomedical Optics* **22**(12), 121606 (2017).

[11] G. C. Keene and M. A. L. Bell, "Assessment of da vinci tool and wrist rotations that maximize fluence in photoacoustic-guided surgery: A simulation study," in *Proceedings of SPIE Photonics West*, SPIE (2025).

[12] R. Lowes, "Crack-prone scissors may burn patients, da vinci maker says." https://www.medscape.com/viewarticle/804067?form=fpf. Accessed: 2024-08-23.

[13] Q. Fang and D. A. Boas, "Monte carlo simulation of photon migration in 3d turbid media accelerated by graphics processing units," *Opt. Express* **17**, 20178–20190 (2009).

[14] J.-P. Ritz, A. Roggan, C. Isbert, *et al.*, "Optical properties of native and coagulated porcine liver tissue between 400 and 2400 nm," *Lasers in Surgery and Medicine: The Official Journal of the American Society for Laser Medicine and Surgery* **29**(3), 205–212 (2001).

[15] P. Parsa, S. L. Jacques, and N. S. Nishioka, "Optical properties of rat liver between 350 and 2200 nm," *Appl. Opt.* **28**, 2325–2330 (1989).

[16] T. Zhao, A. E. Desjardins, S. Ourselin, *et al.*, "Minimally invasive photoacoustic imaging: Current status and future perspectives," *Photoacoustics* **16**, 100146 (2019).

[17] I. Surgical, "Instrument and accessory catalog," (2023).

[18] M. A. L. Bell, X. Guo, D. Y. Song, *et al.*, "Transurethral light delivery for prostate photoacoustic imaging," *Journal of Biomedical Optics* **20**(3), 036002 (2015).

[19] D. Ying, "Optical properties of rat liver between 350 and 2200 nm," *iScience* **27** (2024).

[20] A. K. Ustun and J. Zou, "A photoacoustic sensing probe based on silicon acoustic delay lines," *IEEE Sensors Journal* **21**(19), 21371–21377 (2021).

[21] J. Y. Kim, C. Lee, K. Park, *et al.*, "High-speed and high-snr photoacoustic microscopy based on a galvanometer mirror in non-conducting liquid," *Scientific reports* **6**(1), 34803 (2016).

[22] N. Mahmoodian and J. Haddadnia, "A framework of photoacoustic imaging for ovarian cancer detection by galvo-mirror system," *J Bioeng Biomed Sci* **6**(184), 2 (2016).

[23] R. Yao, X. Intes, and Q. Fang, "Generalized mesh-based monte carlo for wide-field illumination and detection via mesh retessellation," *Biomed. Opt. Express* **7**, 171–184 (2016).